Journal of the Meteorological Society of Japan, Vol. 90, No. 5, pp. 737−753, 2012
DOI: 10.2151/jmsj.2012-511

Maintenance Mechanisms of a Precipitation Band Formed along the Ibuki-Suzuka Mountains on September 2–3, 2008

Kazuomi MOROTOMI[1], Taro SHINODA

Hydrospheric Atmospheric Research Center, Nagoya University, Nagoya, Japan

Yukari SHUSSE

National Research Institute for Earth Science and Disaster Prevention, Tsukuba, Japan

Takeharu KOUKETSU, Tadayasu OHIGASHI, Kazuhisa TSUBOKI, Hiroshi UYEDA

Hydrospheric Atmospheric Research Center, Nagoya University, Nagoya, Japan

and

Ichiro TAMAGAWA

River Basin Research Institute, Gifu University, Gifu, Japan

(Manuscript received 28 September 2011, in final form 12 April 2012)

Abstract

A heavy rainfall event occurred along the Ibuki-Suzuka Mountains situated to the west of the Nobi Plain, Japan on September 2–3, 2008. This event was caused by a stationary precipitation band that formed along the mountains with a north-south alignment. This study examines the maintenance mechanism of the precipitation band and describes the characteristics of high rainfall intensity in the band. For this purpose, data from the Japan Meteorological Agency (JMA) radar, JMA wind-profiler radar, and a dual-Doppler analysis from two X-band polarimetric Doppler radars are used. The band stagnated for 13 hours from 12 Japan Standard Time (JST; 9 hours ahead of UTC) on September 2. Its length and width were approximately 100 and 20 km, respectively.

Low-level warm and moist southeasterly winds with equivalent potential temperature greater than 355 K below 1 km impinged on the eastern slope of the mountains and continuously developed precipitation cells. These cells propagated northward by southerly winds above 1 km and contributed to the formation of the precipitation band. The maintenance of the precipitation band can be attributed to a persistent vertical wind shear; that is, the low-level southeasterly and mid-level southerly winds.

The characteristics of high rainfall intensity in the precipitation band is examined by dual-Doppler analysis. Low-level southerly winds with high equivalent potential temperature converged over a microscale wedge-shaped valley that opens southward between the Ibuki-Suzuka Mountains and its branch, the Yoro Mountains aligned north-northwest to south-southeast. The existence of graupel particles near the melting level and a high amount of large raindrops below it, depicted by the polarimetric radar, are possible causes for the increased precipitation in the region.

Corresponding author: Taro Shinoda, Hydrospheric Atmospheric Research Center, Nagoya University, Nagoya 464-8601, Japan.
E-mail: shinoda@rain.hyarc.nagoya-u.ac.jp
1 Present affiliation: Japan Radio Co., Ltd.

1. Introduction

Orography directly affects the distribution and intensity of precipitation (Smith 1979), and therefore, orographic precipitation is influenced by dynamical processes including air flow induced by synoptic

conditions and topography, in addition to microphysical processes. Houze (1993) summarized mechanisms of orographic control over precipitation; they are the seeder-feeder mechanism, upslope condensation, upslope triggering of convection, upstream triggering of convection, thermal triggering of convection, lee-side triggering of convection, and lee-side enhancement of convection.

Convective clouds that develop and persist near mountain regions occasionally cause heavy rainfall and contribute to the occurrence of flash flooding. Doswell et al. (1996) noted that heavy rainfall often occurs when deep precipitation cells organize and propagate repeatedly over a specific area. Mountainous regions sometimes play a crucial role in the formation of a quasi-stationary mesoscale convective system (MCS) that produces heavy rainfall in the region. Numerous studies investigate orographic convective precipitation over isolated mountains such as the island of Hawaii, USA (Smolarkeiwicz et al. 1988); Yaku Island, Japan (Kanada et al. 2000); and Jeju Island, Korea (Lee et al. 2010). However, this study focuses on orographic convective precipitation over mountain chains.

Yoshizaki et al. (2000) pointed out that heavy orographic rainfall events are often produced over the upslope or upstream areas of mountain regions through orographic blocking, corresponding to the upslope/upstream triggering of convection. A well-known event illustrating upslope triggering of convection is the Big Thompson storm, which occurred adjacent to the Rocky Mountains in Colorado, USA on July 31, 1976. Caracena et al. (1979) found that an orographic uplift of a low-level inflow released convective instability and light winds at steering levels, causing the system to remain over the windward slope and contribute to the formation of the heavy rainfall event. Yoshizaki and Ogura (1988) accurately reproduced the structure of the Big Thompson storm using three-dimensional, high-resolution numerical simulations, and noted that a cold pool plays an important role in maintaining the quasi-stationary structure. Yu et al. (2007) observed upslope triggering precipitation over the windward slopes of the southeastern Alps using an airborne Doppler radar during the intensive observation period (IOP) of the Mesoscale Alpine Programme (MAP). They reported that convective precipitation is formed through the triggering of potentially unstable air through simple upslope lifting. Grossman and Durran (1984) reported significant precipitation west of the Western Ghats Mountains in India through orographic blocking, corresponding to the upstream triggering of convection. Ogura and Yoshizaki (1988) accurately reproduced the convective region over the upstream area of the mountains. Moreover, orographic enhancement of precipitation was investigated over mountainous regions in Japan. Kikuchi et al. (1988) reported that the enhancement mechanism is the upslope triggering of convection in addition to microscale convergence over the valleys in the Orofure mountain range in Hokkaido.

Chu and Lin (2000) investigated the effects of orography on the generation and propagation of precipitation systems over a mesoscale mountain using an idealized two-dimensional cloud-resolving model. They showed that three regimes are identified by the unsaturated moist Froude number ($F_w = U/N_w H$; U is the upstream wind speed, N_w is the unsaturated Brunt-Väisälä frequency, and H is the mountain height). In regime (I) of the low F_w, an upstream propagating precipitation system is formed. In regime (II) of the moderate F_w, a quasi-stationary convective system over the vicinity of the mountain peak is formed. In regime (III) of the high F_w, two modes of precipitation systems are identified: the quasi-stationary and downstream propagation modes. Chen and Lin (2005) expanded their study and showed that four regimes are identified by combination of F_w and convective available potential energy (CAPE). The quasi-stationary precipitation system over the vicinity of the mountain peak develops under conditions of low F_w and CAPE. To investigate the orographic precipitation system, the relationship of precipitation systems to the atmospheric environment shown by their studies should be confirmed observationally.

Lin et al. (2001) proposed four common ingredients for producing heavy orographic rainfall, including (1) a convectively unstable airstream impinging on a mountain, (2) a very moist low-level jet (LLJ), (3) a steep mountain, and (4) a quasi-stationary synoptic condition. A deep, short-wave trough or high CAPE plays an important role in the formation of heavy rainfall around a mountainous region with concave geometry, which favors convection triggering. In addition, Lin (2007) arranged them into nine common ingredients; they are (1) high precipitation efficiency of the incoming airstream, (2) a LLJ, (3) steep orography, (4) favorable (concave) mountain geometry and a confluent flow field, (5) strong synoptically forced upward vertical motion, (6) a moist unstable low-level flow, (7) a high moisture flow upstream, (8) presence of a large, preexisting convective system, and (9) slow or impeded movement of the convective system.

In these common ingredients, many studies point out that the moist LLJ plays an important role to the

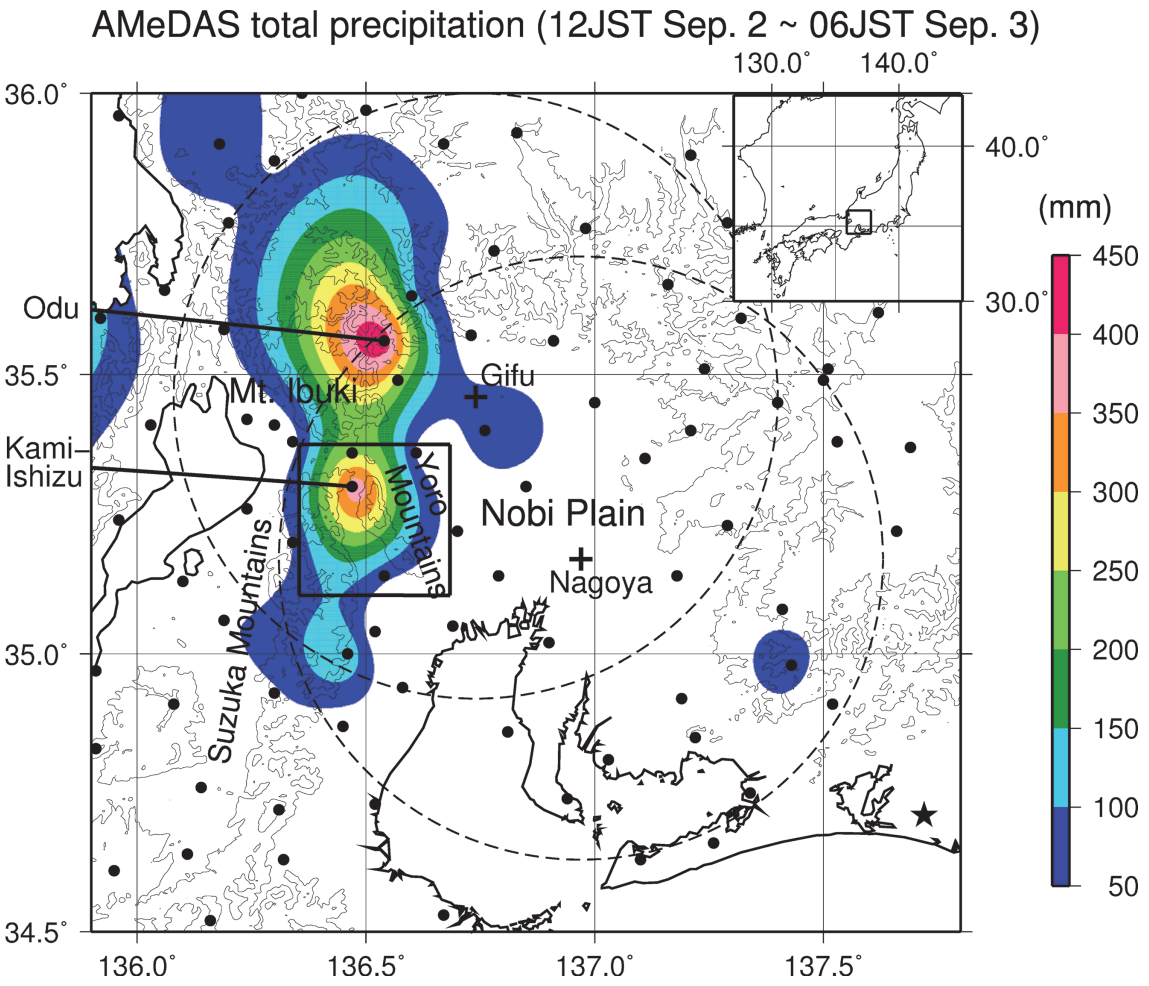

Fig. 1. Horizontal distribution of total precipitation amount from 12 JST on September 2 to 06 JST on September 3, 2008, as obtained by the AMeDAS. Points indicate AMeDAS stations. Contours show ground heights of 300 and 600 m. Crosses and dashed circles represent the locations of the X-band polarimetric radars at Nagoya and Gifu universities and their observation ranges (61.8 km). A rectangle represents the dual-Doppler analysis area shown in Fig. 11a. A star indicates the location of the upper-air sounding station (Hamamatsu) shown in Fig. 6.

precipitation enhancement over the windward slopes by its orographic lifting, in particular, in the vicinity of tropical cyclones (Sakakibara 1979; Lin et al. 2001; Lin et al. 2002; Wu et al. 2002; Lin et al. 2005; Yu and Cheng 2008). However, the maintenance mechanism of precipitation systems producing heavy rainfall without the LLJ around a mountain chain has never been investigated.

A mountain chain composed of Mt. Ibuki and the Suzuka Mountains, called as the Ibuki-Suzuka Mountains in this study, is located to the west of the Nobi Plain, Japan, as shown in Fig. 1. Its peak height exceeds 1000 m. A heavy precipitation event occurred along the mountains on September 2–3, 2008. The horizontal distribution of accumulated rainfall amount from 12 Japan Standard Time (JST: 9 h ahead of UTC) on September 2 to 06 JST on September 3 obtained by the Automated Meteorological Data Acquisition System (AMeDAS) operated by the Japan Meteorological Agency (JMA) is shown in Fig. 1. The precipitation area is locally concentrated along the mountains. In addition, heavy precipitation is observed near Kami-Ishidu (136.474°E, 35.304°N) and Odu (136.544°E, 35.564°N) stations. The total rainfall amounts are 425.0 mm at Odu and 385.0 mm at Kami-Ishidu for 18 hours beginning at 12 JST on September 2 (Fig. 2).

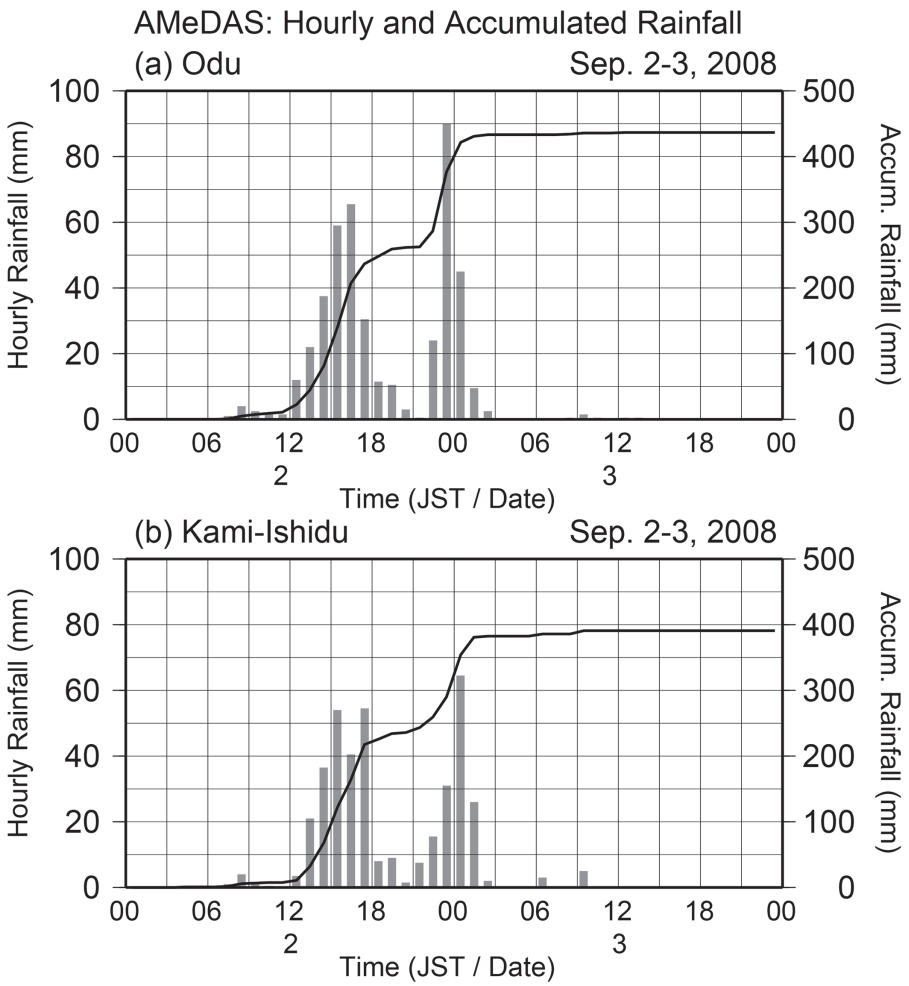

Fig. 2. Time series of hourly rainfall amounts (bar graph) and accumulated amounts (solid lines) observed at (a) Odu and (b) Kami-Ishidu AMeDAS stations from 00 JST on September 2 to 24 JST on September 3, 2008.

The hourly rainfall amounts reaches 90.0 mm at Odu from 23 JST to 24 JST on September 2 and 65.0 mm at Kami-Ishidu from 00 JST to 01 JST on September 3.

Figure 3 shows the horizontal distribution of rainfall intensity at 0000 JST on September 3, 2008 obtained by the JMA radar. The precipitation system formed a band maintained for 13 hours from 12 JST on September 2 to 01 JST on September 3. The purpose of this study is to examine the maintenance mechanisms of the band-shaped precipitation system along the mountains using data obtained by the JMA C-band precipitation radar and wind-profiler radar. In addition, high rainfall intensity was observed near the Kami-Ishidu station. This study also describes the characteristics of high rainfall intensity in the band by dual-Doppler analysis using two X-band polarimetric Doppler radars.

An overview of the observations is given in Section 2. Synoptic situations during the heavy rainfall event are presented in Section 3. Observational results on the maintenance mechanisms of the precipitation band and the characteristics of high rainfall intensity in the band are shown in Section 4. In Section 5, the maintenance mechanisms of the precipitation system are discussed, and a summary is presented in Section 6.

2. Observation data

To clarify the maintenance mechanism of the precipitation band along the mountains and to describe the characteristics of high rainfall intensity in the band, data obtained by X-band polarimetric Doppler radars located at Nagoya University (136.97°E, 35.17°N) and Gifu University (136.74°E, 35.46°N) were used. Table

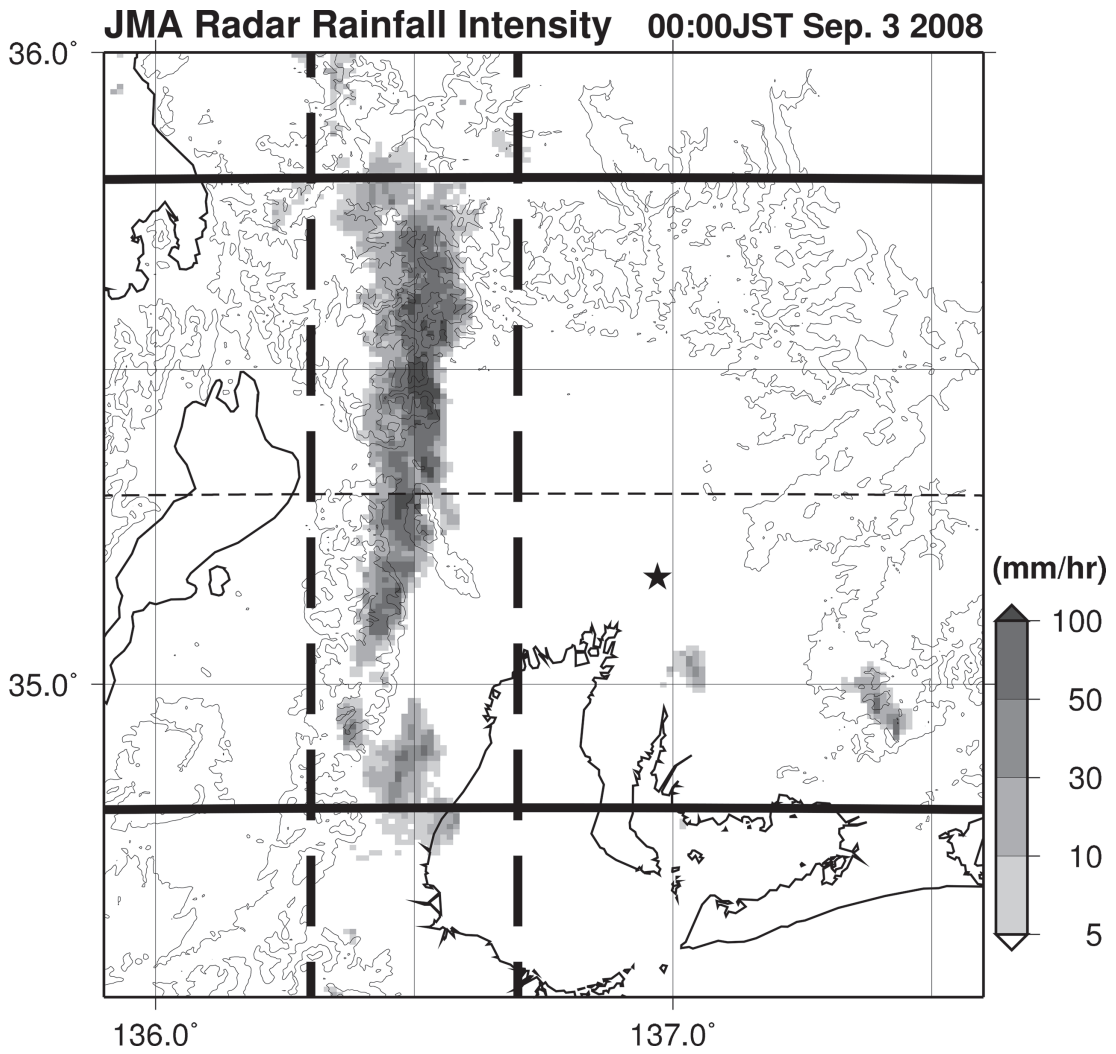

Fig. 3. Horizontal distribution of rainfall intensity (shading) at 0000 JST on September 3, 2008 obtained by the JMA radar. Contours show heights of 300 and 600 m. A star indicates the location of Nagoya Local Meteorological Observatory. Dashed and solid lines indicate the ranges of longitude-time and time-latitude sections presented in Figs. 7, 8. A thin dashed line represents the topography along 35.3°N in Fig. 7.

1 summarizes the system parameters of the radars: a solid-state-type transmitter is operated simultaneously with horizontal (H-) and vertical (V-) polarization signals, and H- and V-independent digital receivers are used. The radars are able to obtain horizontal radar reflectivity (Z_h), Doppler velocity, differential reflectivity (Z_{dr}), differential propagation phase (Φ_{dp}), correlation coefficient between H- and V-polarization signals (ρ_{hv}), and specific differential phase (K_{dp}). The detailed explanation of these parameters is presented in Bringi and Chandrasekar (2001). Z_h and Z_{dr} are corrected for rainfall attenuation using K_{dp} shown by Jameson (1992). Sampling resolutions are 150 m and 1.2° in the direction of the beam and azimuth, respectively. Radius of the observation range is 61.8 km.

Plan position indicator (PPI) data are collected at a dual pulse repetition frequency (PRF) of 1600 and 2000 Hz. The number of integration pulses is 104 Hz for 1600 Hz PRF and 130 Hz for 2000 Hz. The rotation rate of the PPI scans is 3.0 rpm, which obtains three-dimensional (3D) volume scans with 13 elevation angles 0.5°–27.6° in 6-min intervals during the precipitation event.

All polarimetric parameters are interpolated to a

Table 1. System parameters of the X-band polarimetric Doppler radars located at Nagoya and Gifu universities.

Frequency	9415 MHz at Nagoya Univ. 9375 MHz at Gifu Univ.
Peak power	200 W
Pulse width	32μs
PRF	1600–2000 Hz (Dual)
Antenna diameter	2.0 m (parabolic)
Beamwidth	< 1.2°
Antenna gain	> 41 dB
Sidelobe level	< –43 dB
Antenna scan speed	PPI: 4.0 rpm (max.) PPI: 3.0 rpm (obs.)
Polarization	Horizontal (H) and vertical (V)

Cartesian grid volume using a weighting function (Cressman 1959). The grid spacings are 0.5 km in both horizontal and vertical directions. Three-dimensional wind fields in precipitation regions are calculated by dual-Doppler analysis using the method developed by Gao et al. (1999).

In addition, this study uses the JMA radars and the AMeDAS data every 10 min. The JMA C-band precipitation radar data depict the horizontal distribution of rainfall intensity at a height of 2 km with a horizontal grid resolution of 1 km. Data obtained in 10-min intervals by a wind-profiler radar located at Nagoya Local Meteorological Observatory are used to analyze the vertical profile of horizontal winds.

3. Synoptic condition

The surface weather chart at 21 JST on September 2 is shown in Fig. 4. A stagnant depression was located around 135°E, 32°N near the western coastline of Japan. The chart indicates that the target region, including the mountains shown in Fig. 1, is located to the north of the depression. Figure 5 shows the time series of the horizontal distributions of equivalent potential temperature (θ_e) and winds near the surface from 09 JST on September 2 to 03 JST on September 3, which was obtained by the JMA Mesoscale Model (MSM) data. The high-θ_e airmass, defined by θ_e larger than 350 K, extended over the northwestern Pacific Ocean during the period. At 09 JST on September 2, easterly wind was dominant around the target region (Fig. 5a). At 15 JST and 21 JST on September 2, the high-θ_e airmass intruded into the southern coastal region of the Japan Islands by southeasterly wind advection around the northwestern rim of the depression (Figs. 5b, c). At 03 JST on September 3, wind direction varied southerly around the target region

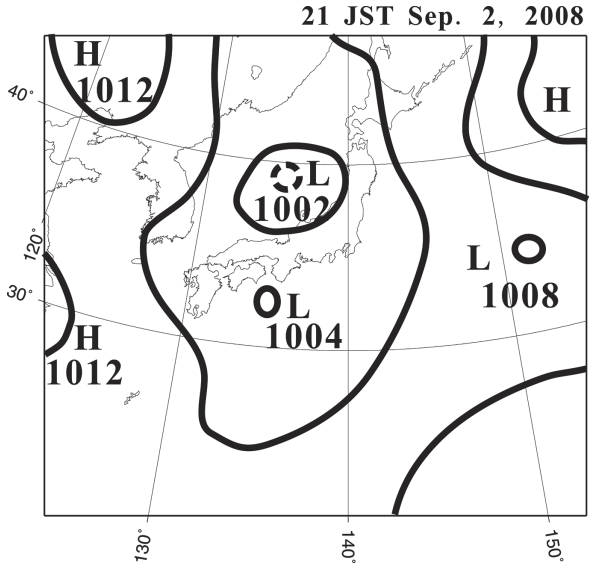

Fig. 4. Surface weather chart at 21 JST on September 2, 2008.

(Fig. 5d).

Figure 6 shows the upper-air sounding observation at Hamamatsu that was located on the windward side of the precipitation band at 21 JST on September 2. Surface θ_e was 357.1 K; convectively unstable stratification appeared below a height of 2 km. The mixing ratio of water vapor around the surface was 19.55 g kg^{-1}; thus, a very moist airmass existed around the surface. Since the moist airmass was present in the lower troposphere, estimated precipitable water was 53.68 kg m^{-2}. The melting level was located at a height of 5.2 km. The estimated lifting condensation level (LCL) and level of free convection (LFC) were approximately 0.65 and 1.0 km, respectively. CAPE and convective inhibition (CIN) calculated using virtual temperature were 1242 and 4.86 J kg^{-1}, respectively. Low LFC, small CIN, and moderate CAPE indicated that moist convection could easily develop from triggering effects, such as the mountains. The LFC was approximately the same as the peak heights of the mountains. The synoptic condition, which persisted during the heavy precipitation event, and the vertical stratification closely resembled those of the Aichi heavy rainfall event on August 28–29, 2008 reported by Shinoda et al. (2012).

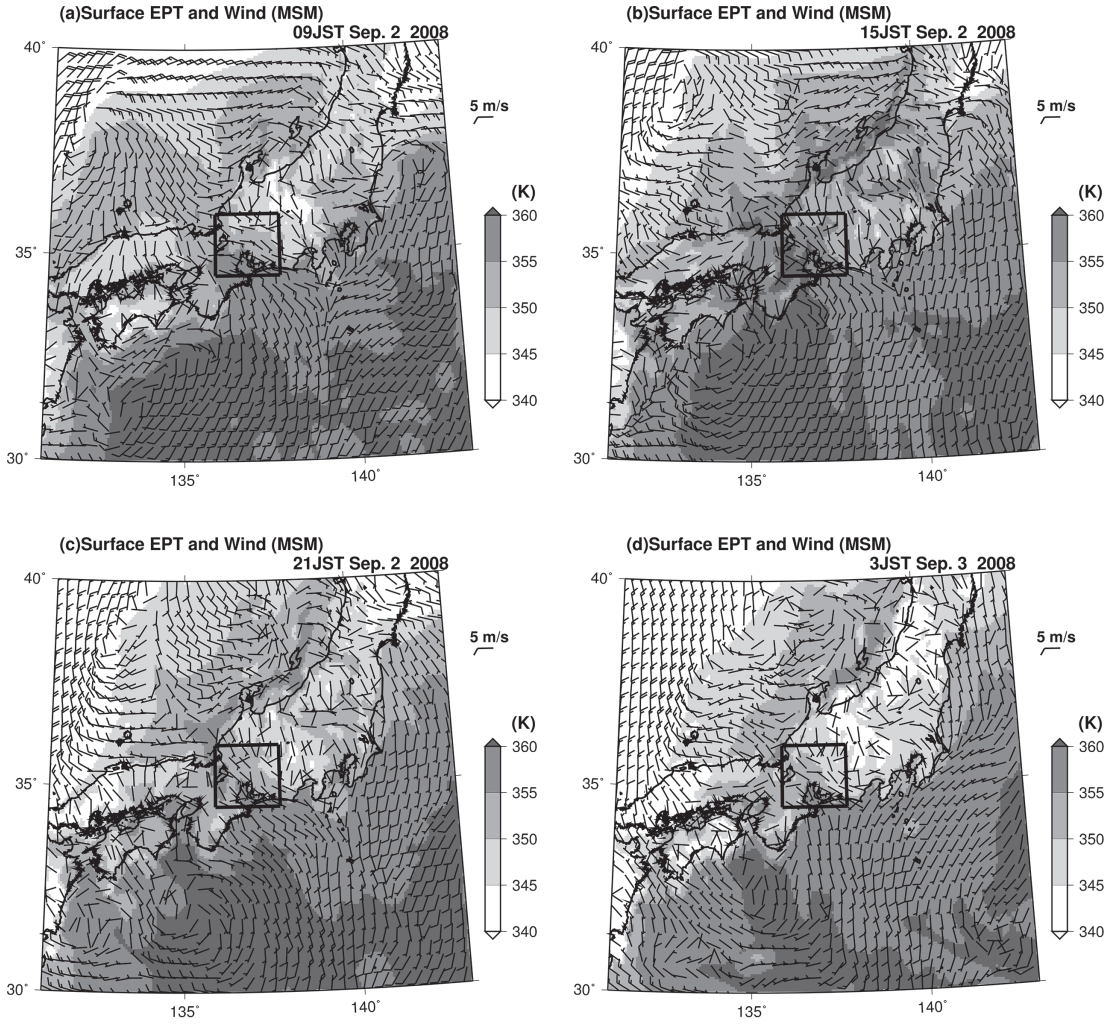

Fig. 5. Horizontal distributions of equivalent potential temperature (shading) and winds (barbs) around the surface (a) at 09 JST, (b) at 15 JST, (c) at 21 JST on September 2, and (d) at 03 JST on September 3, 2008 given by the MSM data. Full- and half-barbs depict 5 and 2.5 m s^{-1}, respectively. Bold rectangle indicates the target region for the present study.

4. Results

4.1 Maintenance mechanisms of the precipitation band

Before 12 JST on September 2, precipitation cells developed randomly over the Nobi Plain and surrounding mountains, propagating northwest-ward (not shown). The precipitation band shown in Fig. 3 initially formed at about 12 JST along the mountains. At 13 JST, its length and width were about 100 and 20 km, respectively. The precipitation band retained its shape and length during its stagnation.

Figure 7 shows a longitude-time section of maximum rainfall intensity between 34.8°N and 35.8°N obtained by the JMA radar. Topography along 35.3°N represented by the thin dashed line in Fig. 3 is shown at the bottom of the figure. Because the Ibuki-Suzuka Mountains are situated approximately along 136.4°E, maximum rainfall intensity above 30 mm h^{-1} was maintained over the eastern slope of the mountains from about 12 JST on September 2 to 01 JST on September 3. The precipitation band was stagnant in the east-west direction for about 13 hours. After 01 JST on September 3, the precipitation area propagated east-

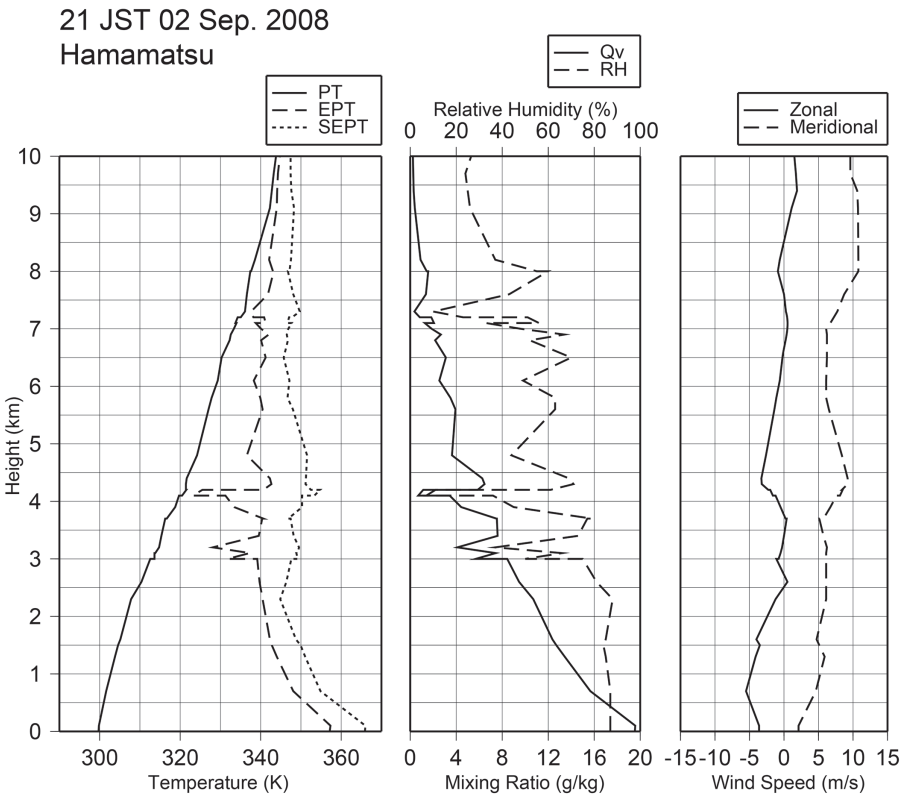

Fig. 6. Vertical profiles obtained by an upper-air sounding at Hamamatsu at 21 JST on September 2, 2008, indicating potential temperature (PT; solid line in the left panel), equivalent potential temperature (EPT; broken line in the left panel), saturated equivalent potential temperature (SEPT; dotted line in the left panel), mixing ratio of water vapor (Qv; solid line in the center panel), relative humidity (RH; broken line in the center panel), zonal wind speed (solid line in the right panel), and meridional wind speed (broken line in the right panel).

ward at approximately 3.0 m s^{-1}.

Figure 8 shows a time-latitude section of maximum rainfall intensity between 136.3°E and 136.7°E obtained by the JMA radar. Topography ranging from 136.3°E to 136.7°E in the longitudinal direction and from 34.0°N to 36.0°N in the latitudinal direction is shown in the left side of Fig. 8. This longitudinal range corresponded to the continuous intense rainfall shown in Fig. 7. The continuous intense rainfall area corresponding to the stagnant precipitation band extended between 34.8°N and 35.8°N. In the precipitation band, significant rainfall intensity regions above 100 mm h^{-1} that would correspond to precipitation cells appeared to propagate northward at speeds 4.8–12.0 m s^{-1}.

To confirm the propagation of precipitation cells in the band-shaped system, data of the X-band polarimetric Doppler radar located at Nagoya University were used. Figure 9a shows the horizontal distribution of reflectivity at a height of 3 km at 1230 JST on September 2. The time series of vertical cross sections in maximum reflectivity in the east-west direction projected on the north-south axis in the rectangular region shown in Fig. 9a is presented in Fig. 9b. Several precipitation cells detected in the cross sections propagated northward in the precipitation band. For example, a precipitation cell located at about 15 km at 1206 JST propagated northward and reached 35 km at 1248 JST. The propagation speed of precipitation cells was estimated to be 6.5–8.0 m s^{-1}, corresponding to that shown in Fig. 8.

To investigate the relationship between the maintenance of the precipitation band and the atmospheric environment, Fig. 10 captures a time series of horizontal winds in a vertical profile observed by the wind-profiler radar located at Nagoya Local Meteorological Observatory. Since Nagoya is located to the east

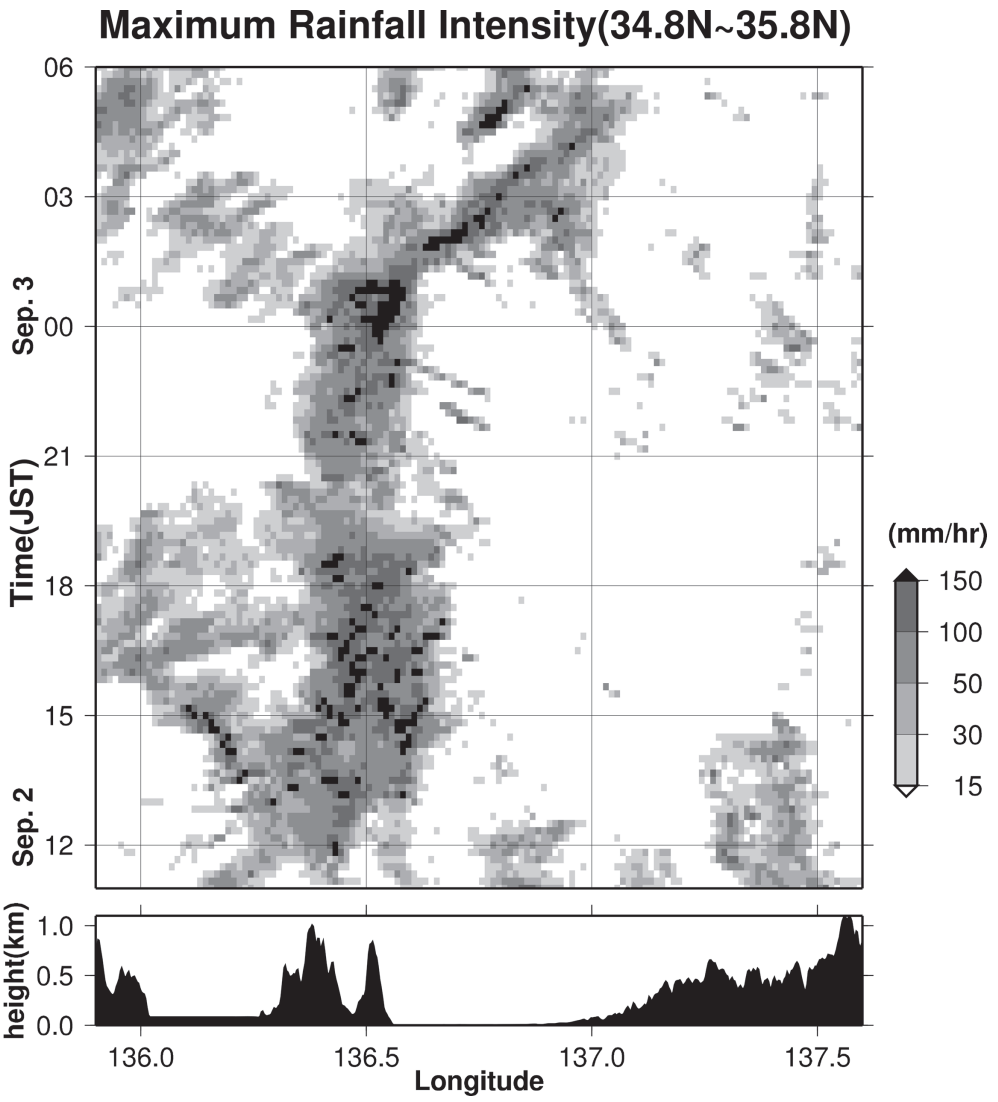

Fig. 7. Longitude-time section of maximum rainfall intensity between 34.8°N and 35.8°N (ranged by solid lines in Fig. 3) obtained by the JMA radar from 1140 JST on September 2 to 0600 JST on September 3, 2008. Maximum rainfall intensity in the latitudinal direction is projected on the longitudinal axis at each observation time of the JMA radar. Topography along 35.3°N is shown in the bottom illustration (represented by the thin dashed line in Fig. 3).

of the precipitation band, the horizontal winds in the vertical profiles should be considered as those of the windward side of the precipitation band. As shown in Fig. 7, the precipitation band formed at about 12 JST on September 2 and remained until about 01 JST on September 3. During the period, low-level southeasterly winds at approximately 5 m s^{-1} were dominant below a height of 1 km and expected to be high-θ_e airmasses, as shown in Figs. 5, 6. The time series of low-level winds corresponded to that of horizontal distributions around the target region shown in Fig. 5. Thus, low-level southeasterly winds could supply warm and moist airmasses to provide suitable conditions for the continuous development of precipitation cells over the eastern slope of the mountains.

At about 11 JST on September 2, easterly wind components between 1 and 2 km in height reduced; thus, the wind direction changed from southeasterly to

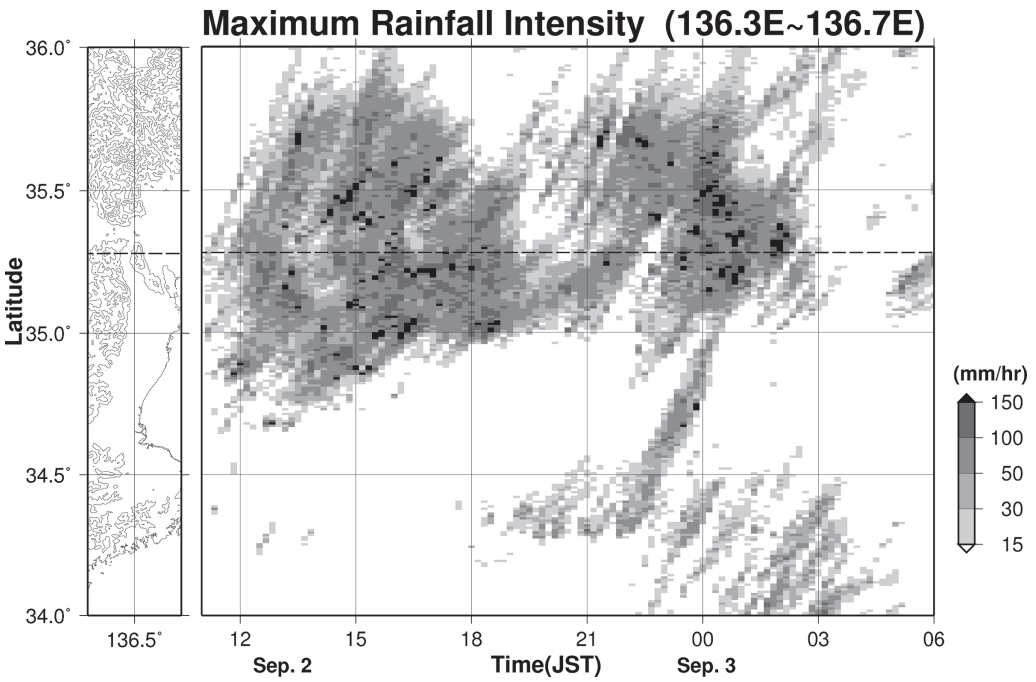

Fig. 8. Time-latitude section of maximum rainfall intensity between 136.3°E and 136.7°E (ranged by broken lines in Fig. 3) obtained by the JMA radar from 1140 JST on September 2 to 0600 JST on September 3, 2008. Maximum rainfall intensity in the longitudinal direction is projected on the latitudinal axis at each observation time of the JMA radar. Topography ranging from 136.3°E to 136.7°E in the longitudinal direction and from 34.0°N to 36.0°N in the latitudinal direction is shown at left.

southerly above a height of 1 km. As shown in Figs. 8, 9b, precipitation cells propagated northward in the band. Thus, it is considered that these precipitation cells formed over the eastern slope of the mountains and moved northward via the mid-level southerly wind above a height of 1 km. The wind-profiler radar revealed that the wind speeds of the mid-level southerly at heights of 2 and 5 km were respectively 4–7 m s^{-1} and 2–5 m s^{-1} during the stagnant period of the precipitation band. Because the northward propagation speed of precipitation cells in the band was 4.8–12.0 m s^{-1}, the cells were expected to be advected by the mid-level southerly wind. As a result, the precipitation band aligned in the north-south direction along the mountains. It is suggested that the precipitation band remained during the period of wind field sustenance by the synoptic atmospheric conditions from 12 JST on September 2 to 00 JST on September 3.

4.2 Characteristics of high rainfall intensity in the band

Significant rainfall intensity above 100 mm h^{-1} was frequently observed in the precipitation band near the Kami-Ishidu station (35.304°N) from 14 JST to 19 JST on September 2 and from 23 JST on September 2 to 01 JST on September 3, as shown in Fig. 8. Figure 9c shows a time series of vertical cross sections of maximum reflectivity from 1700 JST to 1754 JST. During the period, a stagnant precipitation cell with a horizontal scale of approximately 10 km formed around the 35–45 km region. Figure 11a shows the horizontal distribution of radar reflectivity (Z_h) at a height of 3 km and horizontal winds at a height of 1 km near the Kami-Ishidu station at 1730 JST on September 2. This region corresponded to the northern tip of the 30–50 km region shown in Fig. 9c. The high reflectivity region enclosed by the solid rectangle corresponded to the low-level convergence by southerly winds at a height of 1 km. The convergence zone also corresponded to a wedge-shaped valley that opens southward between the Ibuki-Suzuka Mountains, aligned north-south, and its branch, the Yoro Mountains, aligned north-northwest to south-southeast.

Figure 11b shows the vertical cross section of Z_h,

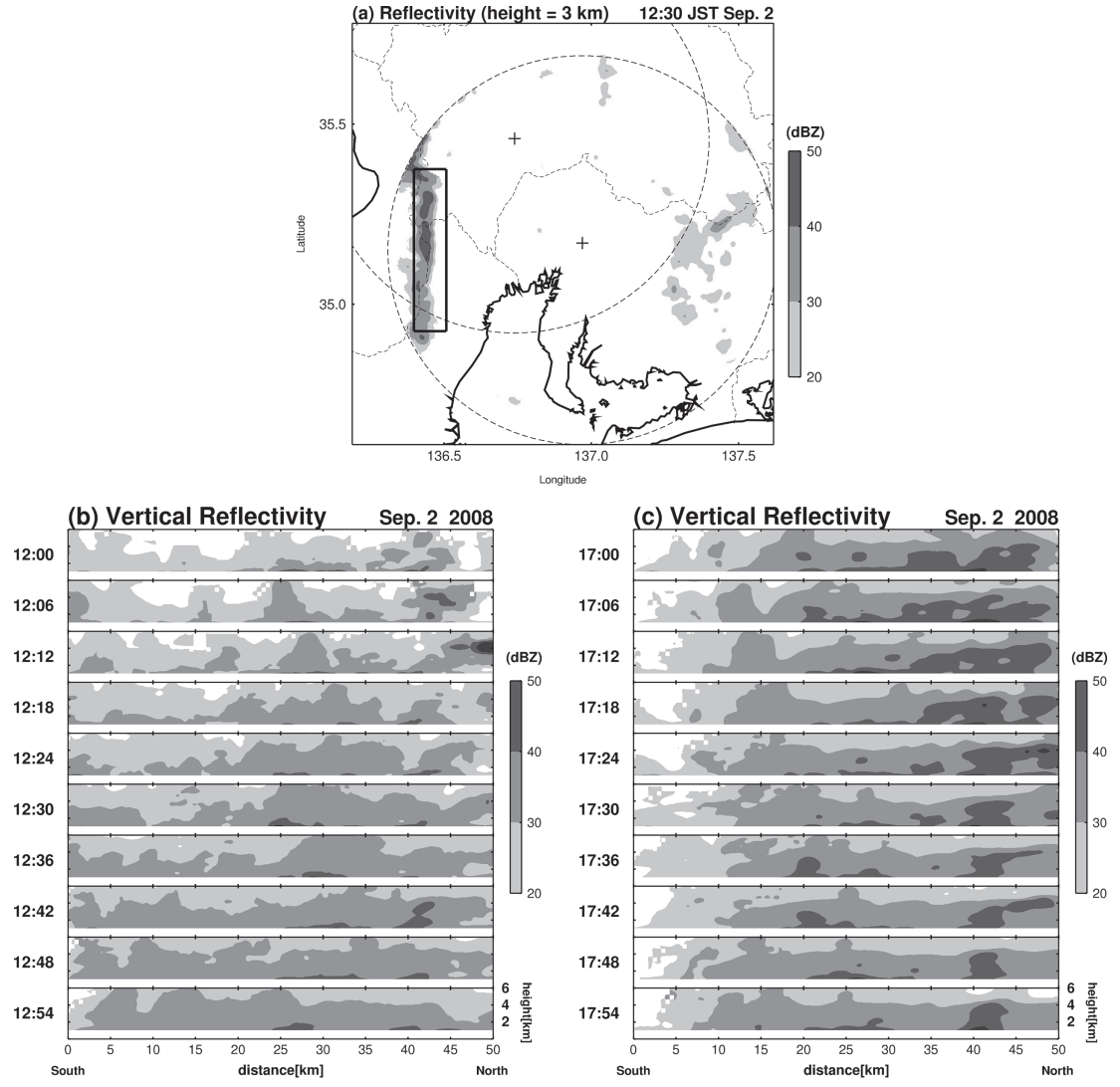

Fig. 9. (a) Horizontal distribution of reflectivity at a height of 3 km at 1230 JST on September 2, 2008 observed by a polarimetric radar located at Nagoya University. (b) Time series of vertical cross sections of maximum reflectivity in the east-west direction projected on the north-south axis in the rectangular region shown in Fig. 9a obtained in 6-min intervals from 1200 JST to 1254 JST on September 2. (c) Same as that described for Fig. 9b, but from 1700 JST to 1754 JST on September 2. Crosses and dashed open circles indicate the location of the X-band polarimetric Doppler radars at Nagoya and Gifu universities and their observation ranges.

wind vectors, and vertical velocity along the A-B plane shown in Fig. 11a. An updraft region at heights between 2.5 and 6.0 km with maximum velocity of approximately 4 m s^{-1} located at a distance of 9 km should be induced by the low-level convergence. A strong downdraft region at heights between 2.0 and 6.5 km with a maximum velocity of approximately 6 m s^{-1} appeared in a different precipitation cell located at a distance of 15 km. Figure 11c shows the vertical cross section of differential reflectivity (Z_{dr}) along the same plane as that shown in Fig. 11b. The regions of high Z_{dr} corresponded to those of high Z_h; that is, precipitation cells. The maximum Z_{dr} was greater than 3.5 dB in one precipitation cell located at a distance of 15 km. A high value of Z_{dr} suggests the existence of large raindrops below the melting level (5.2 km). On the other

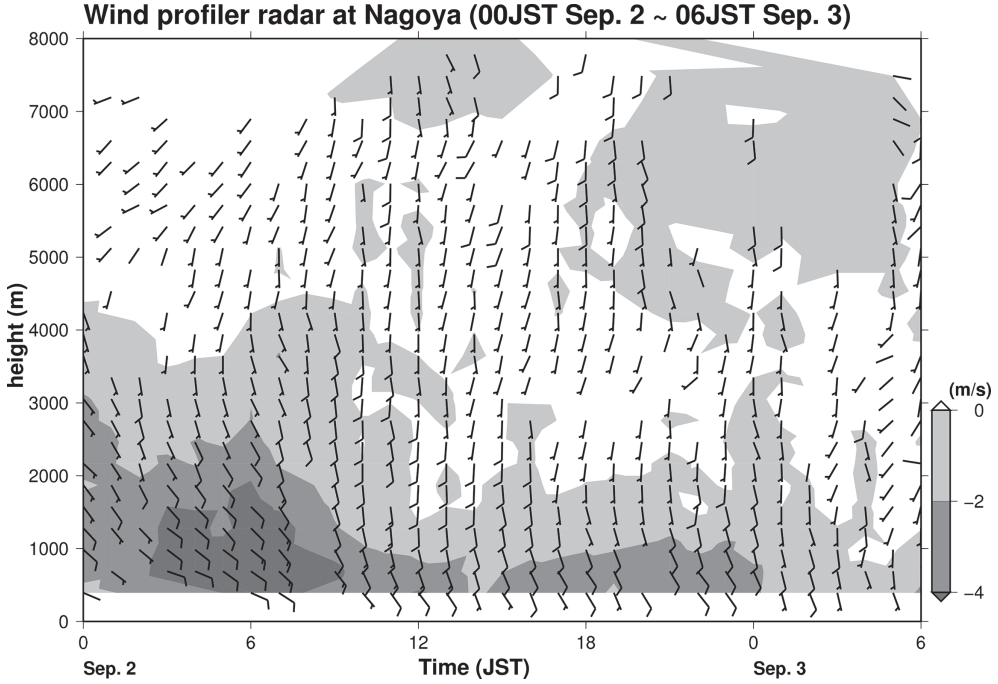

Fig. 10. Time series of horizontal winds in a vertical profile observed by a wind-profiler radar located at Nagoya Local Meteorological Observatory from 0000 JST on September 2 to 0600 JST on September 3, 2008. Full- and half-barbs indicate 5 and 2.5 m s^{-1} , respectively. Light, moderate, and dark shading represent easterly wind components larger than 0, 2, and 4 m s^{-1}, respectively.

hand, negative regions of Z_{dr} appeared near the melting level, which were above the high Z_{dr} regions. Because Z_h value in the high Z_{dr} region was also greater than 35 dBZe, the existence of well-developed graupel particles is suggested.

Using the polarimetric radar data, Liu and Chandrasekar (2000) developed a particle identification method using fuzzy logic. Although the original method was developed for the S-band radar, it was applied to data obtained by the X-band radar in this study. The original membership functions for Z_h, Z_{dr}, ρ_{hv} , and a modified membership function for K_{dp} applied to the X-band were used to conduct particle identification. The vertical temperature profile obtained by the upper-air sounding observation at Hamamatsu was also used for particle identification. The method of particle identification used in the present study was described by Kouketsu and Uyeda (2009).

Figure 11d shows the vertical distribution of particle identification along the same plane as that shown in Fig. 11b. Wet graupel was identified near the melting level; rain was identified below the melting level. Thus, it is hypothesized that the melting of graupel particles formed large raindrops below the melting level and caused a large amount of rainfall in the precipitation cells.

Figure 12 shows the time series of area-averaged divergence at a height of 1 km in the rectangular region, corresponding to the area of the wedge-shaped valley shown in Fig. 11a. Time series of rainfall amount at Kami-Ishidu and lightning frequency in the rectangular region are also drawn every 10 min. Lightning frequency was obtained by the Lightning Location System (LLS) operated by Chubu Electric Power Co., Inc. Divergence value was not calculated if the grid number of available horizontal wind was less than 60% of that in the rectangular region in Fig. 11a. Convergence appeared from 14 JST to 15 JST and from 16 JST to 19 JST on September 2 and from 23 JST on September 2 to 01 JST on September 3. These periods corresponded to significant rainfall at the Kami-Ishidu station. Lightning frequency increased from 17 JST to 19 JST and from 00 JST to 01 JST, corresponding to the convergence and significant rainfall periods. On the other hand, divergence appeared from 21 JST to 22 JST on September 2. This period corresponded to weak

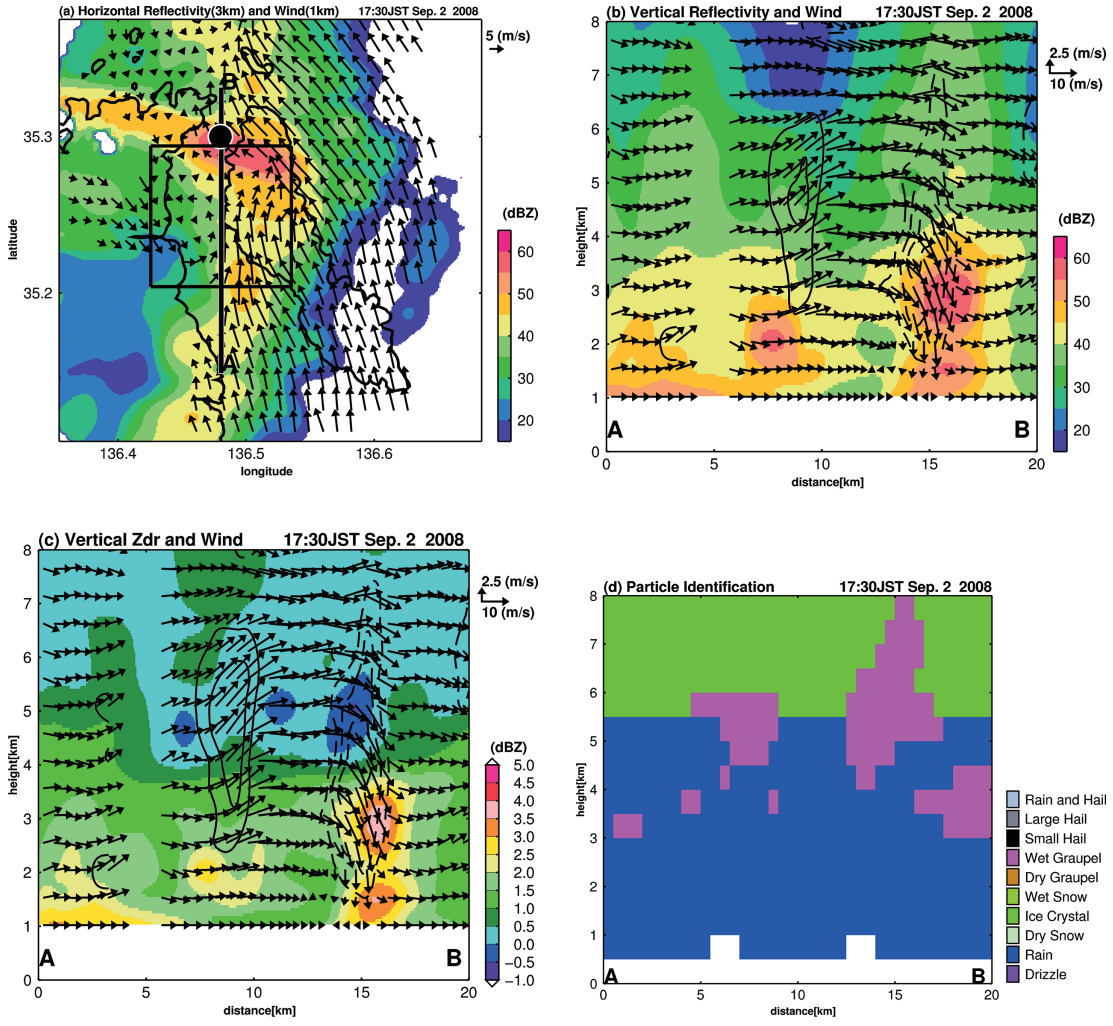

Fig. 11. (a) Horizontal distribution of reflectivity at a height of 3 km (colors) and horizontal winds at a height of 1 km (arrows) in the rectangle shown in Fig. 1 at 1730 JST on September 2, 2008 as observed by polarimetric Doppler radars located at Nagoya and Gifu universities. Contour shows the ground level at 300 m, and a solid rectangle shows an area that calculates divergence shown in Fig. 12. (b) Vertical cross section of reflectivity (colors), wind vectors (arrows), and vertical velocity (contours) along the A-B plane shown in (a). Solid (dashed) contours show updraft (downdraft) regions drawn by every 2 m s^{-1} from ± 2 m s^{-1}. (c) Same as that described for (b), but for differential reflectivity (colors). (d) Same as that described for (b), but for particle identification (colors) without wind vectors and vertical velocity.

rainfall at the Kami-Ishidu station. Also, lightning was not observed during the period.

5. Discussion

5.1 Maintenance mechanisms of the precipitation band

The maintenance mechanism of the precipitation band can be explained by the following factors. (1) A low-level warm and moist southeasterly wind with θ_e greater than 350 K impinged on the Ibuki-Suzuka Mountains aligned north-south, and precipitation cells would develop over the eastern slope of the mountains. The precipitation band located in the vicinity of the mountain peak (Fig. 7). The characteristics closely resembled that of the upslope triggering of convection shown by Houze (1993) and the quasi-stationary precipitation system over a mountain peak (regime II) shown by Chu and Lin (2000). (2) Precipitation cells

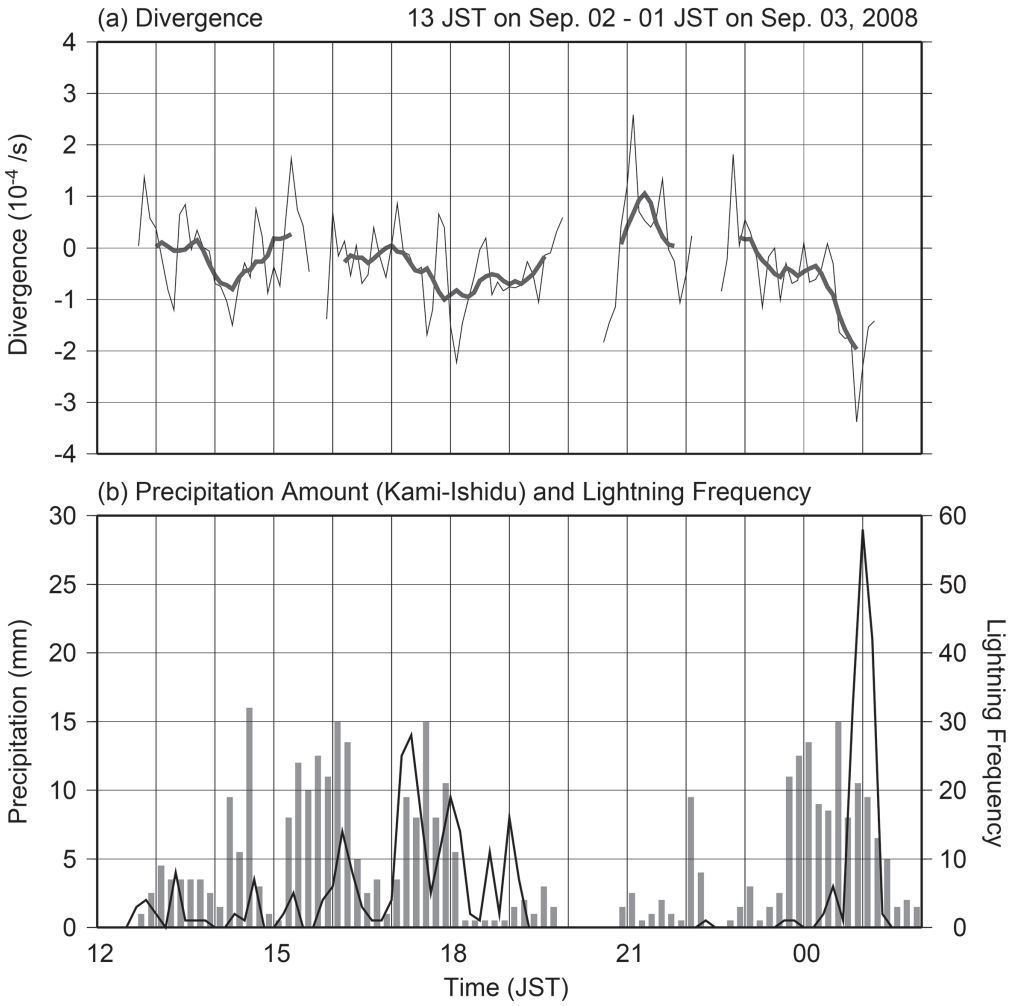

Fig. 12. (a) Time series of area-averaged divergence at a height of 1 km (thin solid line at 6-min intervals) and its moving mean prior to and following three volume scans (bold solid line) in the rectangle shown in Fig. 11a from 12 JST on September 2 to 02 JST on September 3, 2008. The total 36-min average values are indicated as moving mean. Divergence value is not calculated if the grid number of the available horizontal wind is less than 60%. Negative value implies convergence. (b) Time series of 10-min rainfall amounts at the Kami-Ishidu AMeDAS station (bar graph) and that of 10- min accumulated lightning frequencies in the rectangle shown in Fig. 11a observed by the LLS (solid line) are drawn.

propagated northward. The propagation could be attributed to the southerly winds above a height of 1 km. As a result, the precipitation band aligned north-south, corresponding to the alignment of the mountains. This shows that the precipitation band did not have a two-dimensional structure perpendicular to the mountains. (3) The precipitation band was maintained for 13 hours by a sustained wind field in the lower and middle troposphere through quasi-stationary synoptic conditions.

The unsaturated moist Froude number is defined as $F_w = U/N_wH$ (Chu and Lin 2000), where U is the upstream zonal wind speed (perpendicular to the mountains), 3.9 m s^{-1} ; N_w is the unsaturated Brunt-Väisälä frequency, 0.0084 s^{-1}; and H is the mountain height, 1000 m. Here, U and N_w were calculated by the upper-air sounding observation at Hamamatsu. The unsaturated moist Froude number was 0.464. In addition, CAPE was 1242 J kg^{-1}, a moderate value as shown by Chen and Lin (2005). The unsaturated moist

Froude number in the present case was larger than that corresponding to the formation of the regime II (ranging between 0.341 and 0.354) shown by Chu and Lin (2000). They pointed out that the quasi-stationary precipitation system in the vicinity of a mountain peak is attributed to the balance between the moist incoming flow and the cold pool induced by the system. The cold pool was not observed by the AMeDAS network during the persistence of the band-shaped system over the mountains. The lack of cold pool should be attributed to the high humid environment in the lower and middle troposphere shown in Fig. 6. This is the first difference from the result shown by Chu and Lin (2000).

Chu and Lin (2000) used an idealized two-dimensional cloud-resolving model and uniform horizontal wind vertically. In the present case, the three-dimensional structure was characteristic of the band-shaped precipitation system in which precipitation cells propagated northward along the system and the mountains. The structure would be formed by the favorable conditions of the vertical wind shear. This is the second difference from the result shown by Chu and Lin (2000). The precipitation system stagnated in the vicinity of the mountains peak, although these differences appeared in comparison with the previous study shown by Chu and Lin (2000).

After 01 JST on September 3, the wind direction below a height of 1 km changed from southeasterly to southerly (Fig. 10). At that time, the stagnation of the precipitation band ended and it propagated eastward at about 3.0 m s^{-1} (Fig. 7). The unsaturated moist Froude number during the period should be significantly reduced because the upstream zonal wind speed in the lower troposphere was approximately O (0.1) m s^{-1}. This should correspond to the upstream propagating precipitation system from the mountain peak (regime I) shown by Chu and Lin (2000). During the passage of the precipitation band, surface precipitation and a decrease in surface temperature of about 3°C were observed at several AMeDAS stations located on the eastern side of the mountains (not shown). This result suggests that the precipitation band propagated with a weak cold pool; that is, an organized gravity-current-like structure, rather than the orographic effect, contributed to the eastward propagation of the precipitation system.

The common ingredients for producing heavy orographic rainfall proposed by Lin et al. (2001) and Lin (2007) are examined in the present case. The stagnant precipitation band was one of the major ingredients. A warm and moist southeasterly airstream intruded into the target region and impinged on the mountains, the airmass was convectively unstable below a height of 2 km and the CAPE value was 1242 J kg^{-1} , as shown in Figs. 5, 6. The gradient of the eastern slope is approximately 5.5° ; that is, horizontal and vertical scales of the mountains are approximately 10 and 1 km, respectively. Low-level southeasterly and mid-level southerly winds were maintained for 13 hours during the precipitation period (Fig. 10) through the persistence of the synoptic conditions (Fig. 5). However, the approximate wind speeds in the lower troposphere, observed by upper-air sounding (Fig. 6) and the wind-profiler radar (Fig. 10), were 3–8 m s^{-1}. Thus, the existence of LLJ could not be recognized during the precipitation event. Also, a preexisting precipitation system could not be recognized. These results show that almost all of Lin's common ingredients do not need to be satisfied to produce heavy rainfall in a certain area if some ingredients are fully satisfied. In this case, the heavy rainfall event occurred without LLJ and a preexisting precipitation system. These should be important signatures in the present case. These ingredients should be confirmed in other heavy rainfall events.

5.2 Characteristics of high rainfall intensity in the band

As shown in Fig. 1, two peaks of precipitation obtained by the AMeDAS appeared during the event, one at the Kami-Ishidu station (35.30°N) and the other at the Odu station (35.56°N). As shown in Fig. 8, highly frequent high rainfall intensity was located near the Kami-Ishidu station. As shown in Figs. 1, 3, a wedge-shaped valley that opens southward appears around the Kami-Ishidu station. Since the low-level convergence appeared around the region (Fig. 12), a low-level warm and moist inflow converged over the microscale wedge-shaped valley area. The convergence of a high-θ_e airmass was continuously expected to form updrafts and precipitation cells over the wedge-shaped valley and contribute to heavy rainfall there. The additional Lin's gradients that was the "concave mountain geometry and a confluent flow field" should contribute to the high rainfall intensity in the region.

The existence of graupel in the precipitation system was suggested through particle identification via the polarimetric radar near the Kami-Ishidu station (Fig. 11d). Frequent lightning (Fig. 12) also suggested the existence of graupel above the melting level. An active riming process induced by a supply of abundant water vapor and cloud droplets in the high-θ_e southeasterly wind in the lower troposphere could be expected (Figs. 5, 6). The melting of graupel particles that produced

large raindrops coupled with the insignificant evaporation rate owing to the moist environment possibly caused the high amount of rainfall. Thus, the additional Lin's ingredient that was the "high precipitation efficiency" by the hydrometeor concentration through the riming process might also act to increase the rainfall amount in the region. This microphysical process of heavy rainfall induction was similar to that of the Aichi heavy rainfall event on August 28–29, 2008 as proposed by Shinoda et al. (2012).

6. Conclusions

A heavy rainfall event occurred along the Ibuki-Suzuka Mountains situated to the west of the Nobi Plain, Japan on September 2–3, 2008. This event was caused by a stationary precipitation band that formed along the mountains with a north-south alignment. This study examines the maintenance mechanisms of the precipitation band and describes the characteristics of high rainfall intensity in the band. For this purpose, data obtained by the JMA radar, JMA wind-profiler radar, and dual-Doppler analysis from two X-band polarimetric Doppler radars located at Nagoya and Gifu universities were used. This stationary precipitation band aligned in the north-south direction, which corresponded to that of the mountains. The band stagnated along the mountains for 13 hours from 12 JST on September 2. Its length and width were approximately 100 and 20 km, respectively.

Low-level warm and moist southeasterly winds with θ_e greater than 355 K below a height of 1 km impinged on the eastern slope of the mountains and continuously developed precipitation cells. These cells propagated northward by the southerly winds above a height of 1 km, corresponding to the alignment of the precipitation band and the mountains. The maintenance mechanism of the precipitation band can be attributed to the persistence of the vertical wind shear; that is, low-level southeasterly and mid-level southerly winds persisted for about 13 hours by synoptic conditions.

The characteristics of high rainfall intensity in the precipitation band were examined by dual-Doppler analysis. This analysis reveals that low-level southerly winds with high-θ_e converged over a microscale wedge-shaped valley that opens southward between the Ibuki-Suzuka Mountains and its branch, the Yoro Mountains, aligned north-northwest to south-southeast. The convergence of a high-θ_e airmass was continuously expected to form updrafts and precipitation cells, causing heavy rainfall over the region, although the causal relationship between the low-level convergence and convection. In these precipitation cells, the existence of graupel near the melting level and a high amount of large raindrops below it were suggested by data obtained by the polarimetric radar. The hydrometeor concentration through the riming process by graupel particles was also expected to increased precipitation amount in the region.

Acknowledgements

The authors express their gratitude to Mr. M. Kato and other members of the Laboratory of Meteorology, Hydrospheric Atmospheric Research Center, Nagoya University for their useful comments. The authors thank Mr. A. Sakakibara, Chuden CTI Co., Ltd. for his providing the lightning (LLS) data. We are also grateful to Dr. D. P. Jorgensen and three anonymous reviewers for their fruitful comments. This study was supported by formation of a virtual laboratory for diagnosing the Earth's climate system (VL), defrayed by the Ministry of Education, Culture, Sports, Science and Technology of Japan. Upper-air sounding data were obtained from the website of the University of Wyoming (Atmospheric Soundings). Figures were drawn using the Generic Mapping Tools (GMT).

References

Bringi, V. N., and V. Chandrasekar, 2001: *Polarimetric Doppler Weather Radar.* Cambridge University Press, 636 pp.

Caracena, F., R. A. Maddox, L. R. Hoxit, and C. F. Chappell, 1979: Mesoanalysis of the Big Thompson storm. *Mon. Wea. Rev.*, **107**, 1–17.

Chen, S.-H., and Y.-L. Lin, 2005: Effects of moist Froude number and CAPE on a conditionally unstable flow over a mesoscale mountain ridge. *J. Atmos. Sci.*, **62**, 331–350.

Chu, C.-M., and Y.-L. Lin, 2000: Effects of orography on the generation and propagation of mesoscale convective systems in a two-dimensional conditionally unstable flow. *J. Atmos. Sci.*, **57**, 3817–3837.

Cressman, G. P., 1959: An operational objective analysis system. *Mon. Wea. Rev.*, **87**, 367–374.

Doswell, C. A., III, H. E. Brooks, and R. A. Maddox, 1996: Flash flood forecasting: An ingredients-based methodology. *Wea. Forecasting*, **11**, 560–581.

Gao, J., M. Xue, A. Shapiro, and K. K. Droegemeier, 1999: A variational method for the analysis of three-dimensional wind fields from two Doppler radars. *Mon. Wea. Rev.*, **127**, 2128–2142.

Grossman, R. L., and D. R. Durran, 1984: Interaction of low-level flow with the western Ghats Mountains and offshore convection in the summer monsoon. *Mon. Wea. Rev.*, **112**, 652–672.

Houze, R. A., Jr., 1993: *Cloud Dynamics.* Academic Press, 573pp.

Jameson, A. R., 1992: The effect of temperature on attenuation correction schemes in rain using polarization propagation differential phase shift. *J. Appl. Meteor.*, **31**, 1106–1118.

Kanada, S., H. Minda, B. Geng, and T. Takeda, 2000: Rainfall enhancement of band-shaped convective cloud system in the downwind side of an isolated island. *J. Meteor. Soc. Japan*, **78**, 47–67.

Kikuchi, K., N. Horie, T. Harimaya, and T. Konno, 1988: Orographic rainfall events in the Orofure mountain range in Hokkaido, Japan. *J. Meteor. Soc. Japan*, **66**, 125–139.

Kouketsu, T., and H. Uyeda, 2009: Trial of hydrometeor classification in a thundercloud in Nobi Plain, Japan using multiparameter radar. *Prep. of Conference on MCSs and High-Impact Weather/Climate in East Asia (Seoul Korea)*, 276–281.

Lee, K.-O., S. Shimizu, M. Maki, C.-H. You, H. Uyeda, and D.-I. Lee, 2010: Enhancement mechanism of the 30 June 2006 precipitation system observed over the northwestern slope of Mt. Halla, Jeju Island, Korea. *Atmos. Res.*, **97**, 343–358.

Lin, Y.-L., 2007: *Mesoscale Dynamics.* Cambridge University Press, 646pp.

Lin, Y.-L., S. Chiao, T.-A. Wang, M. L. Kaplan, and R. P. Weglarz, 2001: Some common ingredients for heavy orographic rainfall. *Wea. Forecasting*, **16**, 633–660.

Lin, Y.-L., D. B. Ensley, S. Chiao, and C.-Y. Huang, 2002: Orographic influences on rainfall and track deflection associated with the passage of a tropical cyclone. *Mon. Wea. Rev.*, **130**, 2929–2950.

Lin, Y.-L., S.-Y. Chen, C. M. Hill, and C.-Y. Huang, 2005: Control parameters for the influence of a mesoscale mountain range on cyclone track continuity and deflection. *J. Atmos. Sci.*, **62**, 1849–1866.

Liu, H., and V. Chandrasekar, 2000: Classification of hydrometeors based on polarimetric radar measurements: Development of fuzzy logic and neuro-fuzzy systems, and in situ verification. *J. Atmos. Oceanic Technol.*, **17**, 140–164.

Ogura, Y., and M. Yoshizaki, 1988: Numerical study of orographic-convective precipitation over the eastern Arabian Sea and the Ghats Mountains during the summer monsoon. *J. Atmos. Sci.*, **45**, 2097–2122.

Sakakibara, H., 1979: Cumulus development on the windward side of a mountain range in convectively unstable air mass. *J. Meteor. Soc. Japan*, **57**, 341–348.

Shinoda, T., M. Kato, Y. Shusse, M. Nomura, M. Oue, T. Ohigashi, K. Tsuboki, and H. Uyeda, 2012: Structure of a precipitation system developed around Aichi Prefecture, Japan on 28–29 August 2008: Analysis using an X-band polarimetric radar and a cloud-resolving model. *Mon. Wea. Rev.*, submitted.

Smith, R. B., 1979: The influence of mountains on the atmosphere. *Advances in Geophys.*, **21**, 87–230.

Smolarkeiwicz, P. K., R. M. Rasmussen, and T. L. Clark, 1988: On the dynamics of Hawaiian cloud bands: Island forcing. *J. Atmos. Sci.*, **45**, 1872–1905.

Wu, C.-C., T.-H. Yen, Y.-H. Kuo, and W. Wang, 2002: Rainfall simulation associated with Typhoon Herb (1996) near Taiwan. Part I: The topographic effect. *Wea. Forecasting*, **17**, 1001–1015.

Yoshizaki, M., and Y. Ogura, 1988: Two- and three-dimensional modeling studies of the Big Thompson storm. *J. Atmos. Sci.*, **45**, 3700–3722.

Yoshizaki, M., T. Kato, Y. Tanaka, H. Takayama, Y. Shoji, H. Seko, K. Arao, K. Manabe, and Members of X-Baiu-98 Observation, 2000: Analytical and numerical study of the 26 June 1998 orographic rainband observed in western Kyushu, Japan. *J. Meteor. Soc. Japan*, **78**, 835–856.

Yu, C.-K., and L.-W. Cheng, 2008: Radar observations of intense orographic precipitation associated with Typhoon Xangsane (2000). *Mon. Wea. Rev.*, **136**, 497–521.

Yu, C.-K., D. P. Jorgensen, and F. Roux, 2007: Multiple precipitation mechanisms over mountains observed by airborne Doppler radar during MAP IOP5. *Mon. Wea. Rev.*, **135**, 955–984.